Characterization of Cross-Linking Depth for Thin Polymeric Films Using Atomic Force Microscopy

Qiuquan Guo,[1] Maxim Paliy,[1,2] Brad Kobe,[2] Tomas Trebicky,[1,2] Natalie Suhan,[3] Gilles Arsenault,[3] Lorenzo Ferrari,[3] Jun Yang[1]

[1]Mechanical and Materials Engineering, Western University, London, Ontario N6A 5B9, Canada
[2]Western Surface Science, Western University, London, Ontario N6A 5B9, Canada
[3]Lanxess Inc, 999 Collip Circle, London, Ontario N6G 4X8, Canada
Correspondence to: J. Yang (E-mail: jyang@eng.uwo.ca)

ABSTRACT: Thin polymeric films made with various elastomers, like polyisoprene, and elastomer composites were prepared for characterization of cross-linking depth in this study. Various cross-linking methods have been applied to get mechanically stronger, more thermally stable and chemically resistant polymer coatings. However, there is no existing approach that could effectively characterize the degree or depth of cross-linking for thin polymer films. The objective of this work is to use atomic force microscopy to characterize cross-linking depth in a precise way. Hyperthermal hydrogen bombardment-induced cross-linking was employed as a cross-linking method and the depth of cross-linking was estimated via local change of the elastic modulus along the sample cross-section with precise force measurement and high spatial resolution. It is found that the cross-linking depth is closely related to the chemical composition of thin films. Understanding the depth of cross-linking is vital for a broad range of applications. It is believed that the developed technique is also applicable for studying other cross-linkable materials. © 2014 Wiley Periodicals, Inc. J. Appl. Polym. Sci. **2015**, *132*, 41493.

INTRODUCTION

Cross-linking is widely used to promote desired changes of physical properties of various polymeric materials. Cross-linked materials generally possess better performance including mechanical strength, thermal stability, and chemical resistance. This is especially important with the increasing application of membranes or thin films in various industrial areas such as organic thin film electronics,[1,2] gas separation,[3] fuel cell application.[4] It is imperative to develop effective methods for surface modification and functionalization of various membrane materials. More importantly, characterization of the cross-linking with high spatial resolution is crucial for understanding both the cross-linking method and resulted material performance.

Various physical and chemical cross-linking methods have been applied to cure polymers, biomaterials, thin films, etc. A thermal method was developed to prepare chemically resistant membranes for reverse osmosis.[5] Ultraviolet (UV) cross-linking is another popular method for membrane cross-linking.[6] Photograft polymerization method[7,8] was used to achieve bulk polymerization of membranes and also surface functionalization of fabricated devices.[7] Chemically and radiation cross-linked poly-

mers were prepared by radiation graft method for fuel cell application.[9] Chemical cross-linking method[10–12] was used to obtain desired property and better performance of various membranes. Among various cross-linking methods, the hyperthermal hydrogen induced cross-linking (HHIC)[13,14] is a novel and original way of cross-linking organic molecules containing C—H bonds. Traditional methods to cross-link organic materials typically use harsh chemicals and catalysts. The HHIC process is a vacuum based approach that uses a broad and scalable beam of hyperthermal hydrogen molecules to cleave C—H bonds, thus creating free carbon radicals on the surface of a polymer. The carbon radicals subsequently migrate and recombine to produce cross-links not only on the surface of a polymer but also in the bulk up to several microns. The fact that HHIC fundamentally requires no co-agents or solvents together with high throughput and relatively low energy consumption allows us to label it a "green process". The ability to cross-link micron thick layers to stretchable substrates has broad potential in the field of organic electronics and medical device applications.

Note that HHIC is a surface-sensitive technique, capable of controlling the cross-linking depth of a sample from hundreds of nanometers to a few microns.[15] Cross-linking depth is thus a
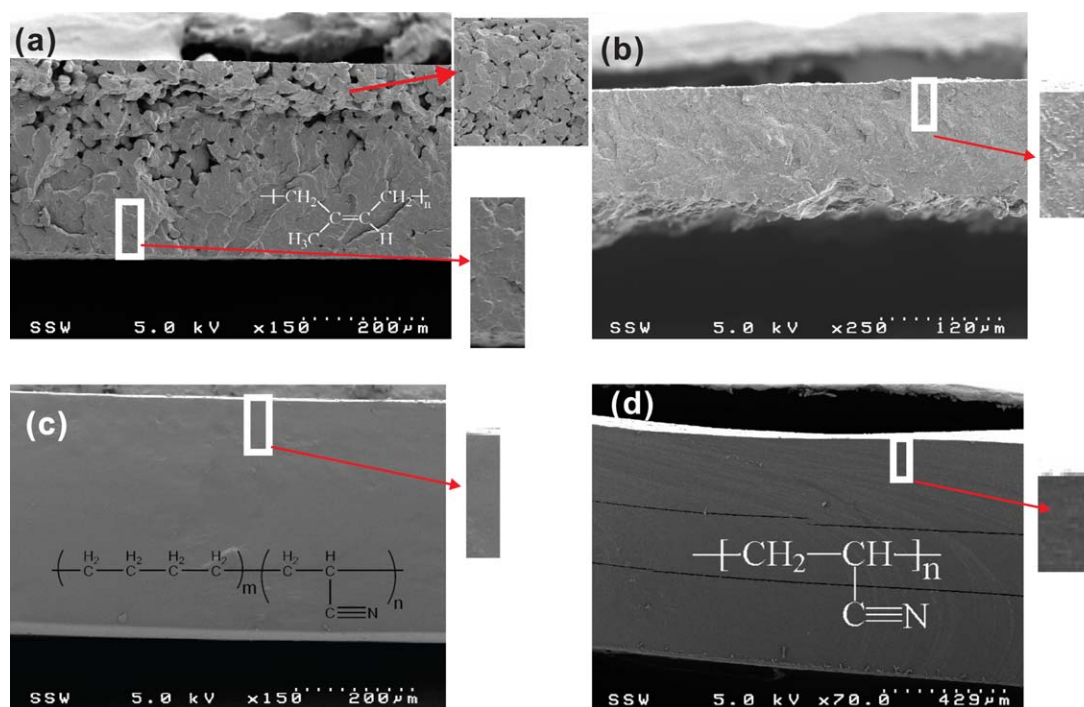
Figure 1. SEM images of thin film samples after HHIC treatment. (a) Pure PIP, (b) PIP/CNT composite, (c) Therban®, and (d) PAN. The rectangle areas are the smooth site chosen for AFM measurements. The white rectangles indicate the flat measurement areas. [Color figure can be viewed in the online issue, which is available at wileyonlinelibrary.com.]

critical parameter to determine the property of cross-linked composite material. Fourier transform infrared (FTIR) spectroscopy can detect functional groups of raw and treated materials to elucidate the cross-linking effect.[5,16,17] X-ray diffraction (XRD) is able to provide the degree of cross-linking by investigating the crystalline structure of materials before and after cross-linking.[12] The swelling test represents another standard method to study the degree of cross-linking through dissolving polymers into proper organic solvent and quantitating gel fraction of the composite membrane.[18,19] For coatings or thin films where only a few nanometers to a few microns of sample surfaces are cross-linked, high spatial resolution is required to characterize the cross-linking in detail. However, most cross-linking characterization methods are only suitable for bulk materials, while none of these methods is easily applicable to thin films.

In this study, atomic force microscopy (AFM)[20] was used to characterize the cross-linking depth of polymeric materials. With its high accuracy in force measurement, AFM has been used to study mechanical properties in various fields, such as biological samples,[21] biomaterials,[22] and polymers.[23] Cross-linked polymers often have strongly different elastic modulus compared to its noncrosslinked counterpart,[24,25] although there is no simple relation between elastic moduli and the density of cross-links. In the present work we presume, though, that the elastic modulus is a monotonically increasing function of the degree of cross-linking. Furthermore, HHIC is employed as the surface-sensitive cross-linking technique. After HHIC, we carefully prepared freeze-fractured cross-sections of thin films for AFM measurements. Then, on the cross-sections, we measured

the elastic moduli of the sample as a function of the distance from the surface. The elastic moduli were calculated from the measured AFM force curves. This innovative technique is quite universal and can be used to characterize the cross-linking thickness of various materials. Since AFM is able to measure the elastic modulus from a small area with nanometer resolution, it could provide detailed cross-linking mappings with high spatial resolution, both in the lateral directions and in the direction normal to the sample surface.

EXPERIMENTAL

Materials
Polyisoprene (PIP) pellets (99+%. *trans*−1,4) and polyacrylonitrile (PAN) were purchased from Sigma-Aldrich. Chloroform (HPLC grade) was purchased from Fisher Scientific. Multiwalled carbon nanotubes (outside diameter: ∼5–15 nm, length: ∼50 μm) were purchased from US Research Nanomaterials. The other polymers like Therban® (HNBR) were supplied by LANXESS. All chemicals were used as received. The molecular weight of PIP, PAN, and Therban® are 400, 150, and 226 kDa respectively.

Preparation of Samples
Thin films of pure PIP, PIP/CNT composite, Therban®, and PAN were prepared for AFM measurements. PIP was dissolved in chloroform uniformly through sonication. The PIP/chloroform solution (15 mg/mL) was then added to a 250 mL glass beaker and evaporated until dry. The resulting thin films were approximately 250 μm thick and were usually porous on the side adjacent to the bottom of the glass beaker [Figure 1(a), top
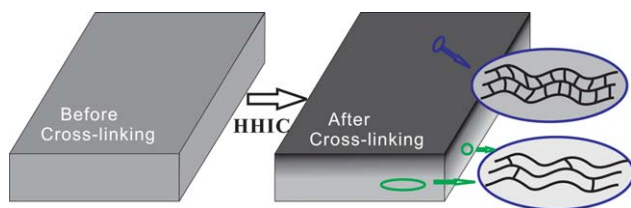
Figure 2. Schematic illustration of the thin films crosslinked with hyperthermal hydrogen-induced cross-linking technique: formation of crosslinked chains induces increase of the stiffness closer to the surface. [Color figure can be viewed in the online issue, which is available at wileyonlinelibrary.com.]

side of the sample]. The generation of this porosity structure is most likely caused by the evaporation of the solvent being blocked by the side adjacent to the bottom of the glass beaker, resulting crystallization of PIP into the *spherulite* structures [inset in Figure 1(a)]. However, the air exposed side resembles that of a typical thin film coating [Figure 1(a), bottom side of the sample] being compact and uniform and this side was used to study the cross-linking depth via AFM.

The PIP/CNT composite samples with 14 wt % of CNT were prepared according to the following procedure. Initially, CNTs were well dispersed in chloroform through sonication and PIP was added into the solution to get 1 mg/mL PIP/CNT in solution. Then CNT/PIP solution in chloroform was evaporated under continuous magnetic stirring until it reached 50 mg/mL overall concentration, and then it was left to fully dry without stirring. The resulting PIP/CNT composite films are compact, nonporous and have uniformly dispersed CNTs. The films are approximately 150 μm thick [Figure 1(b)]. The surface adjacent to the bottom of the glass beaker is very smooth and was used to measure the cross-linking depth.

Therban® (HNBR) [Figure 1(c)] samples were prepared according to the procedure similar to that for pure PIP. However, instead of drying the samples directly on the bottom surface of a glass beaker, a substrate of either polyethylene or vulcanized black-filled butyl rubber was placed in the beaker and used as a scaffold to support the dried films. The resulting films required a scaffold because they did not have the mechanical strength to support their own weight during freeze-fracture cross-sectioning and AFM analysis.

The polyacrylonitrile (PAN) samples [Figure 1(d)] were prepared using similar procedure used to prepare the pure PIP film, while dimethylformamide was used to dissolve PAN instead of chloroform. In addition, the concentration used was 10 mg/mL instead of 15 mg/mL because PAN has a lower solubility. The PAN samples are relatively stiffer and have good quality freeze-fractured cross sections [Figure 1(d)] for AFM analysis.

Cross-Linking Using HHIC Reactor
The samples were cross-linked using a hyperthermal hydrogen-induced cross-linking technique (Figure 2) developed and operated at Surface Science Western. Briefly, an operating pressure of neutral hydrogen was maintained at 0.8 mTorr. Hydrogen ions produced by electron cyclotron resonant plasma were

extracted using an applied potential of −100 V and an extraction current of 10 mA into an electric field-free region. The hydrogen ions then collide with background hydrogen gas molecules to generate hyperthermal neutral projectiles driving the cross-linking reaction on the sample. Above the sample holder, the remaining charged particles were reflected by an applied bias of 100 V (positive ions) and −50 V (electrons). The samples were cross-linked for 10 min.

Preparation of Cross-Sections Using Freeze-Fracture
To obtain flat and uniform cross-sections for AFM analysis, the samples were freeze-fractured using liquid nitrogen ($T = 77$ K) immediately following the HHIC procedure. Samples were cut into rectangular pieces 1 cm × 0.5 cm and immersed in liquid nitrogen for 5 min. The samples were then bent and subsequently fractured while immersed in the liquid nitrogen. Care was taken to ensure that the cross-linked side was on the inside radius and in compression during bending. This was done to avoid stretching and smearing of the cross-section due to the tensile forces on the outside surface of the film. One part of the cross-section, from each freeze-fracture pair, was examined using SEM within the first hour after freeze-fracture to check the quality of the cross-section, and to provide some visual guidance before proceeding with the AFM analysis on the second, complementary part, of the cross-section.

Force Distance Curve Measurement
All experiments were performed on a Dimension V AFM equipped with a Nanoscope controller V (Veeco). A silicon nitride cantilever from Nanoscience with a nominal spring constant of 3 N/m and a tip radius of around 10 nm was used. To achieve more accurate force measurements, the spring constant of the cantilever was calibrated with the thermal tune method[26] and was found to range from 2 to 9 N/m.

The freeze-fracture cross-sections were securely mounted between two pieces of silicon using a SPM cross-sectional sample holder from Bruker AFM. The sample and the AFM cantilever are shown in the AFM optical microscope image presented in Figure 3(a). The cantilever tip can be positioned anywhere on the sample using the Nanoscope controller software (Nanoscope 7.30, Veeco). As shown in Figure 3(a), the tip of the cantilever was aligned with the center of the red crosshairs and an area of interest represented by the green rectangle was selected for scanning using tapping mode AFM. AFM tapping mode was used to measure the morphology. Next, 'Point-and-Shoot' mode of the AFM was used to image an area width of 5 μm. Two or more lines were then drawn over the 5 μm width and separated into 50 points [Figure 3(b)]. Each point was separated by a distance of 100 nm. Force distance (F–D) curves were then captured for all the points and the maximum indention force was set as <100 nN to minimize sample disturbance. A typical F–D curve is shown in Figure 3(c). After finishing the measurement of the first area, the tip was offset to the next area for measurement until the edge of the sample was reached.

F–D Curve Analysis
Several different mechanical models have been developed for analyzing F–D curves obtained by AFM. In this study, the classical Hertz model[27] was used
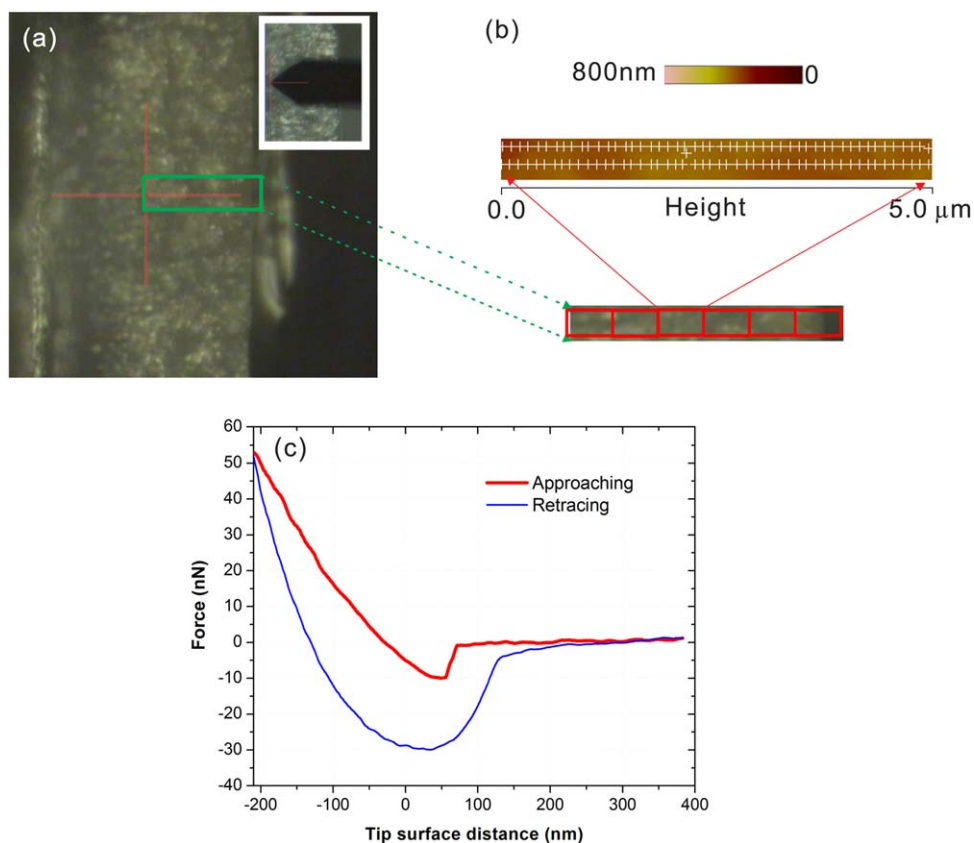
Figure 3. (a) The tip of the cantilever was aligned with the centre of the red crosshairs and an area of interest (green rectangle) was chosen for scanning. (b) Height image of the sample, which was measured from the center to the edge with 5 μm step. For each 5 μm section, at least 2 rows and 50 columns of F–D curves were obtained. (c) A typical F–D curve. [Color figure can be viewed in the online issue, which is available at wileyonlinelibrary.com.]

$$F = \frac{4\sqrt{R_C}}{3} \frac{E}{1-v^2} \delta^{3/2} \qquad (1)$$

where δ, v, R_C, and E indicate the indentation depth or tip surface distance [Figure 3(c)], Poisson's ratio, the tip radius of the cantilever, and elastic modulus. The Poisson's ratio was assigned the universal value for the rubbery materials $v = 0.49$, and 0.45 for PIP/CNT composite. Each F–D curve includes two processes, approaching and retracing. The approaching curve [red one in Figure 2(c)], which is the indentation curve, was used to calculate the Young's modulus. The Young's moduli of all curves were calculated using a custom Matlab code based on the Hertz model in Eq. (1).

RESULTS AND DISCUSSION

It is plausible to expect that the cross-linked material will have different stiffness, compared to the same material which has not been cross-linked. Young's moduli for all measured points were calculated and plotted as a function of the distance to the sample surface in the normal direction (termed the depth in what follows). Young's modulus distribution versus depth for different polymers after HHIC are shown in Figure 4(b–e) as the raw bar plots (gray) as well as the average curves (red). The averaging was done using the second order Savitzky–Golay smoothing method to better demonstrate the technique. Furthermore, as illustrated with the help

of a sketch in Figure 4(a), each Young's modulus value [one column of the bar plot in Figure 4(b–e)] represents an average value of at least two points taken at the same sample depth (an area of ~100 nm in size depth-wise) in one measurement section shown in Figure 3(b). By examining the modulus change versus the depth, we can conclude that the cross-linked part (closer to the surface) has on average much higher Young's modulus values, compared to the noncrosslinked part. In order to define quantitatively the interface between the cross-linked and noncrosslinked parts of the sample, Young's modulus value from the deeper part of the sample [where the modulus is more or less uniform, e.g., the rightmost parts of the graphs in Figure 4(b–e)] was taken as a reference value (E_{ref}) for each bulk noncrosslinked material. The parts of the sample where the averaged measured Young's modulus [red curves in Figure 4(b–e)] exceeded $1.5E_{ref}$, were considered to be cross-linked. Note that Figure 4(c) (PIP/CNT composite) shows a number of spikes of the Young's modulus even in the noncrosslinked (rightmost) part of the sample. These spikes are associated with stiff CNTs and their bundles; certain spikes with extremely high stiffness (>1 GPa) which represents the stiffness of the CNT itself were excluded from analysis altogether. The remaining spikes, however, did not influence the average bulk noncross-linked value of the Young modulus for the CNT/PIP sample. By comparing Figure 4(b) and 4(c), one can see that, due to
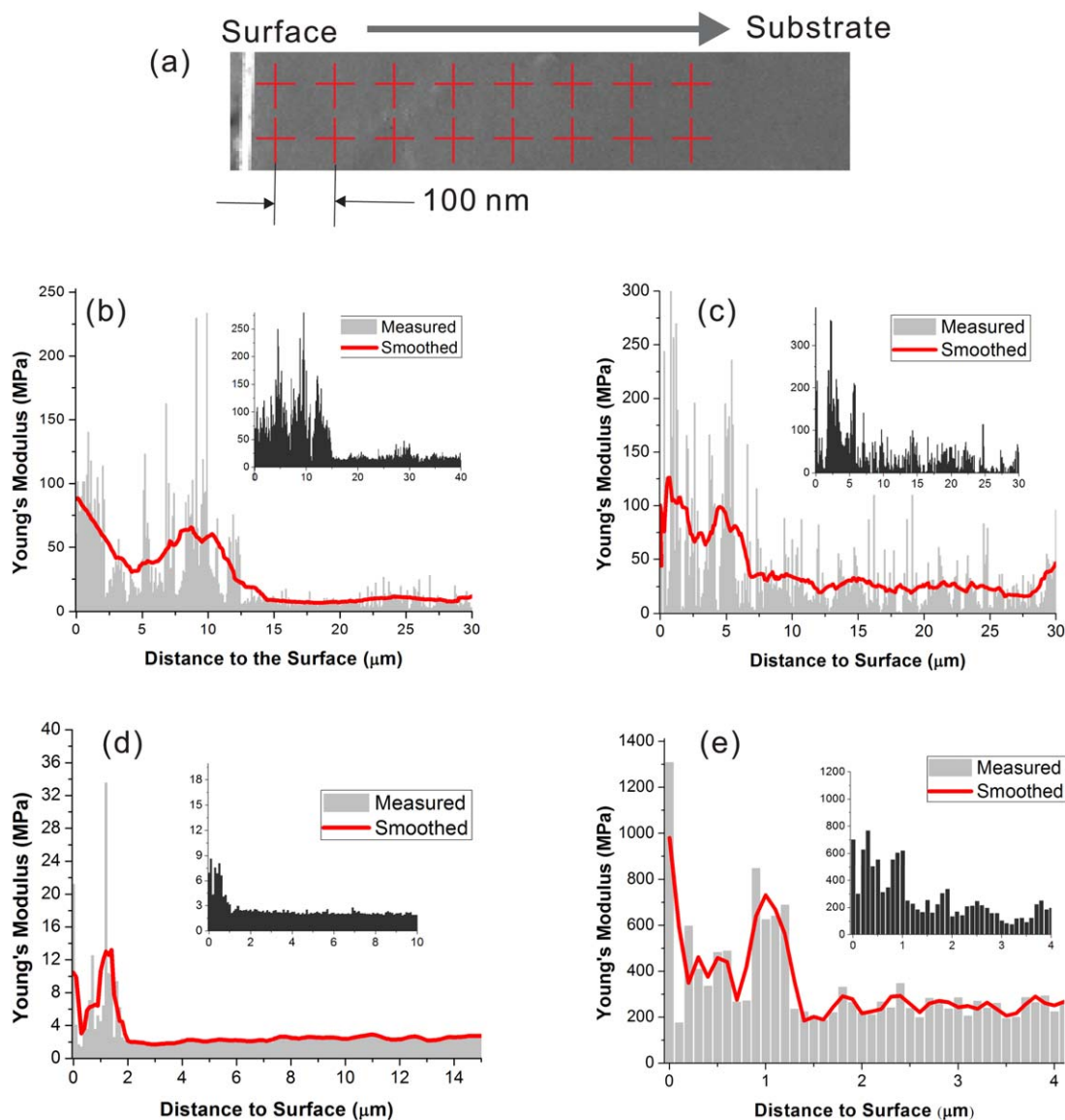
Figure 4. A sketch illustrating the measurement area (a) and typical Young's modulus distribution graphs after HHIC for (b) pure PIP sample, (c) PIP with 14% CNT, (d) Therban® sample, and (e) PAN sample. The insets are another group of measured data for each of the sample. [Color figure can be viewed in the online issue, which is available at wileyonlinelibrary.com.]

the strength enhancement by CNTs, the overall modulus of PIP/CNT composite is noticeably higher than that of pure PIP sample.

With the criterion for cross-linking defined, one can quantitatively determine the cross-linking depth. The average and the standard deviation of the cross-linking depth for all the polymers examined are summarized in Table I (based on a varying number of analyzed samples from 3 to 9). The cross-linking depth of pure PIP is 12.3 ± 2.9 μm; however, the cross-linking depth was found to be lower with the addition of CNTs, namely it is 7.3 ± 0.3 μm for PIP blended with 14% CNTs. The remaining polymers showed much lower cross-linking depth using HHIC technique, compared to PIP. The cross-linking depth of Therban® and PAN has been estimated to be approximately 2.1 and 1.1 μm, respectively. This decrease in cross-linking depth is

attributed to the lack of double bonds being present in these kinds of polymers. It is obvious that both polymers do not have double bond in their molecular structure. Therban® only has ~1–2% of residual double bonds while PAN has even less. In contrast, PIP has abundant C═C double bonds, with one quarter of double bonds on the backbone structure, to facilitate the cross-linking via a "chain reaction" process.[13] Although CNT has abundant of double bonds, these bonds are formed as a large stable conjugated system, which cannot help with the propagation of carbon free radicals. As a result, cross-linking depth of the CNT/PIP composites films is lower compared to the pure PIP films, due to the CNTs preventing the fast propagation of the carbon radicals in the bulk of the sample. If higher cross-linking depth is desired, alternative cross-linking method might be chosen.

Table I. The Cross-Linking Depth for Various Elastomers and Their Composites

Sample	Depth (μm)	Std dev (μm)
PIP	12.3	2.9
PIP + 14% CNT	7.3	0.3
Therban®	<2.1	0.8
PAN	1.1	0.24

It is worth to note that Therban® thin film sample can hardly support its own initial shape due to its low stiffness. Therefore, the prepared sample suffered from "cold flow" which can increase the area of cross-linked part at the cross-section after being freeze fractured. This phenomenon would result in an overestimation of the cross-linking depth for Therban® sample. Although fresh samples were used for AFM analysis in this study, i.e., the time between freeze-fracture and AFM analysis was minimized, the effect of cold flow could not be fully avoided. The wash tests (our separate study, result not listed) have shown that the HHIC efficiency for Therban® and PAN is somewhere around or less than one micron. The result of PAN sample is in accordance with the current study, which again proves that the developed technique can be used to measure submicron size of cross-linking depth.

CONCLUSIONS

By measuring the Young's modulus distribution dependence versus the distance from the sample surface, the cross-linking depth for a range of polymers cross-linked by HHIC method was characterized. The polymers include: PIP(trans), PIP(trans)/CNT composite, Therban®, and PAN, which were carefully chosen to cover a wide range of cross-linking depths by HHIC method. In summary, AFM can be used to measure the cross-linking depth for both pure polymers as well as the polymer composites. PIP(trans) demonstrates the most efficient cross-linking with a depth of approximately 12 μm after 10 min of HHIC exposure, which is attributed to the abundance of carbon double bonds present. However, the addition of MWCNT to the PIP reduced the cross-linking efficiency, due to the shielding effect of the carbon nanotubes. The other two polymers, Therban® and PAN, lack of double bonds, limit the efficiency of cross-linking by HHIC.

In this study, by taking advantage of the change of stiffness for polymeric materials due to cross-linking, we have proposed and developed a useful and efficient AFM-based technique for estimation of the cross-linking depth of the thin films in the range from a few hundred nanometers to several tens of microns with high accuracy. With its high spatial resolution, our technique can provide a method of measuring cross-linking depth that other techniques can hardly achieve. The proposed technique can also be extended to investigate all the thin films having distinguishable mechanical properties induced by other cross-linking treatments.

ACKNOWLEDGMENTS

REFERENCES

1. Klauk, H.; Halik, M.; Zschieschang, U.; Schmid, G.; Radlik, W.; Weber, W. *J. Appl. Phys.* **2002**, *92*, 5259.

2. Dimitrakopoulos, C. D.; Malenfant, P. R. *Adv. Mater.* **2002**, *14*, 99.

3. Qiu, W.; Chen, C.-C.; Xu, L.; Cui, L.; Paul, D. R.; Koros, W. J. *Macromolecules* **2011**, *44*, 6046.

4. Gubler, L.; Gürsel, S. A.; Scherer, G. G. *Fuel Cells* **2005**, *5*, 317.

5. Kim, Y. K.; Lee, S. Y.; Kim, D. H.; Lee, B. S.; Nam, S. Y.; Rhim, J. W. *Desalination* **2010**, *250*, 865.

6. Vanherck, K.; Koeckelberghs, G.; Vankelecom, I. F. J. *Prog. Polym. Sci.* **2013**, *38*, 874.

7. Nakayama, Y.; Matsuda, T.; Irie, M. *ASAIO J.* **1993**, *39*, M545.

8. Wu, G.; Li, Y.; Han, M.; Liu, X. *J. Membr. Sci.* **2006**, *283*, 13.

9. Chen, J.; Asano, M.; Yamaki, T.; Yoshida, M. *J. Power Sources* **2006**, *158*, 69.

10. Charulatha, V.; Rajaram, A. *Biomaterials* **2003**, *24*, 759.

11. Dutczak, S. M.; Cuperus, F. P.; Wessling, M.; Stamatialis, D. F. *Sep. Purif. Technol.* **2013**, *102*, 142.

12. Heydari, M.; Moheb, A.; Ghiaci, M.; Masoomi, M. *J. Appl. Polym. Sci.* **2013**, *128*, 1640.

13. Zheng, Z.; Kwok, W. M.; Lau, W. M. *Chem. Commun.* **2006**, *29*, 3122.

14. Zheng, Z.; Wong, K. W.; Lau, W. C.; Kwok, R. W. M.; Lau, W. M. *Chem. Eur. J.* **2007**, *13*, 3187.

15. Liu, Y.; Yang, D. Q.; Nie, H. Y.; Lau, W. M.; Yang, J. *J. Chem. Phys.* **2011**, *134*, 074704.

16. Fang, B.; Pan, K.; Meng, Q.; Cao, B. *Polym. Int.* **2012**, *61*, 111.

17. Vanherck, K.; Cano-Odena, A.; Koeckelberghs, G.; Dedroog, T.; Vankelecom, I. *J. Membr. Sci.* **2010**, *353*, 135.

18. Yang, Y.-F.; Wan, L.-S.; Xu, Z.-K. *J. Membr. Sci.* **2009**, *326*, 372.

19. Zhou, B.; Pu, H.; Pan, H.; Wan, D. *Int. J. Hydrogen Energy* **2011**, *36*, 6809.

20. Binnig, G.; Quate, C. F.; Gerber, C. *Phys. Rev. Lett.* **1986**, *56*, 930.

21. Guo, Q.; Xia, Y.; Sandig, M.; Yang, J. *J. Biomech.* **2012**, *45*, 304.

22. Leung, K. M.; Wanger, G.; Guo, Q.; Gorby, Y.; Southam, G.; Lau, W. M.; Yang, J. *Soft Matter* **2011**, *7*, 6617.

23. Jee, A.-Y.; Lee, M. *Polym. Test.* **2010**, *29*, 95.

24. Lee, J.; Macosko, C. W.; Urry, D. W. *Macromolecules* **2001**, *34*, 5968.

25. Treloar, L. The physics of rubber elasticity; Clarendon Press: Oxford, **1975**.

26. Hutter, J. L.; Bechhoefer, J. *Rev. Sci. Instrum.* **1993**, *64*, 1868.

27. Hertz, H. *J. Rein. Angew. Math.* **1882**, *92*, 156.